Enhancement of subsurface brain shift model accuracy: a preliminary study

Ishita Garg[a], Siyi Ding[b], Aaron M. Coffey[a], Prashanth Dumpuri[a,b], Reid C. Thompson[a,c], Benoit M. Dawant[a,b], Michael I. Miga*[a,d]

[a]Vanderbilt University, Department of Biomedical Engineering, Nashville, TN
[b]Vanderbilt University, Department of Electrical Engineering, Nashville, TN
[c]Vanderbilt University Medical Center, Department of Neurological Surgery, Nashville, TN
[d]Vanderbilt University Medical Center, Department of Radiology and Radiological Sciences, Nashville, TN

ABSTRACT

Biomechanical models that describe soft-tissue deformations provide a relatively inexpensive way to correct registration errors in image guided neurosurgical systems caused by non-rigid brain shifts. Quantifying the factors that cause this deformation to sufficient precision is a challenging task. To circumvent this difficulty, atlas-based method have been developed recently which allow for uncertainty yet still capture the first order effects associated with brain deformations. More specifically, the technique involves building an atlas of solutions to account for the statistical uncertainty in factors that control the direction and magnitude of brain shift. The inverse solution is driven by a sparse intraoperative surface measurement. Since this subset of data only provides surface information, it could bias the reconstruction and affect the subsurface accuracy of the model prediction. Studies in intraoperative MR have shown that the deformation in the midline, tentorium, and contralateral hemisphere is relatively small. The falx cerebri and tentorium cerebelli, two of the important dural septa, act as rigid membranes supporting the brain parenchyma and compartmentalizing the brain. Accounting for these structures in models may be an important key to improving subsurface shift accuracy. The goals of this paper are to describe a novel method developed to segment the tentorium cerebelli, develop the procedure for modeling the dural septa and study the effect of those membranes on subsurface brain shift.

Keywords: Localization and tracking technologies, image-guided therapy, modeling, neurosurgical procedure, brain shift, finite element modeling, dural septa, tentorium cerebelli, falx cerebri.

1. INTRODUCTION

Image guidance is the standard of care for the surgical treatments of central nervous system neoplasia, epilepsy and cerebrovascular disorders. The fidelity of image to physical space registration, that drives the neurosurgical image guidance system, is known to be compromised by the phenomenon of brain shift, a non-rigid deformation of brain tissue caused by gravity, edema, hyperosmotic drugs administered prior to surgery and tissue resection. This problem was studied by Nauta using framed stereotaxic device and intraoperative CT to find shift of the order of 5mm in tumor resection case[1]. Hill et. al. studied brain tissue deformation after dura opening and before tumor resection and found displacements greater than 1 mm[2]. Other systematic studies to characterize this deformation were performed with the aid of intraoperative imaging modalities and different studies found that the range of deformation for brain tissue could vary from 1cm to 2.5 cm from their pre-operative state during surgery[2-4]. A trained neurosurgeon is aware of the misalignment between the surgical field and the preoperative image and compensates for it to some extent[5] but it is not always possible to accurately predict the amount of shift.

*Phone: 615-343-8336, Fax: 615-343-7919, Email: Michael.I.Miga@vanderbilt.edu, http://bmlweb.vuse.vanderbilt.edu

Extensive work has been reported in literature to compensate for brain shift. Various intraoperative imaging techniques have been employed to correct for brain shift (CT[6], MRI[3] and ultrasound[7]) but their widespread use has been hampered by modality specific limitations. CT has concerns for radiation exposure, MRI requires special surgical instruments and extremely expensive and ultrasound suffers from low soft tissue contrast. Advances in MRI field have permitted the acquisition of rich information preoperatively such as functional imaging, diffusion weighted imaging or angiography. Surgical constraints do not permit reacquisition of that data intraoperatively[8]. Also the intraoperative MR images have a lower signal to noise ratio because the magnet strength is typically weaker than preoperative MR machines. The brain shift literature has shown a general move towards updating the preoperative images rather than using the intraoperative images directly for guidance. Hata et. al. used non-rigid registration between preoperative and intraoperative MR images with a mutual information metric[9]. 3D volumetric non-rigid registration does not have a closed form solution and can be quite computationally intensive, making it unsuitable for use within the surgical timeframe. Biomechanical models using discretized methods (such as finite element techniques) have been explored by many groups for this problem. Hagemann et. al. performed a 2D analysis using a linear elastic model driven by surface displacements computed using active contours method[10]. Ferrant et. al. followed a similar approach and extracted the surface of the cortex and ventricles for the preoperative and intraoperative MR images and used an iterative shape matching algorithm to compute the surface displacements[11]. The surface displacements were used as boundary conditions in a linear elastic model to obtain the volumetric displacements. Wittek et. al. obtained displacement information from intraoperative MR data and obtained volumetric displacement by applying a nonlinear model[12]. Clatz et. al. used a block matching algorithm instead of surface information to drive the model[13]. Blocks were selected based on their intensity variance and they provided subsurface displacement information as well. A hybrid interpolation and approximation technique was used to compute the dense displacement field. All of the above listed methods require an intraoperative MR scan and as previously discussed, those devices are not widely available in the operating rooms due to high cost of operation.

A more cost effective alternative to volumetric intraoperative images is to use sparse data, which wouldn't necessitate the installation of expensive tomographic devices in the OR. Stereoscopic cameras and laser range scanners are two devices in this category. They have been used by different groups to capture cortical surface data to measure intraoperative brain shift. The former involves a pair of charge-couple device (CCD) cameras attached to the stereoscopic microscope. Triangulation is used between corresponding homologous points to estimate the surface coordinates. Skrinjar et. al. and Sun et. al. used this technique to compute intraoperative brain shift[14, 15]. Alternatively, Audette et. al. used a laser range scanning (LRS) device with a non-rigid 2D spline based iterative closest point (ICP) algorithm to register the LRS data to the MR cortical data[16]. Sinha et. al. used a surface mutual information technique to register the LRS data to the MR textured surface[17]. Cao et. al. performed a systematic comparative study of different registration techniques to register physical space and preoperative MR image space[18]. The authors compared feature point based registration, vessel contour ICP based registration, and the Surface MI method developed in Sinha et. al[17]. They also extended the latter method with an additional constraint of high correspondence confidence, and found that overall it provided the most robust registration results. Registration between serial LRS images (before and after tumor resection) was studied by Sinha et. al. using a non-rigid surface registration technique[19]. This work was extended by Ding et. al., who obtained an improvement in mean target registration error using a semi-automatic vessel contour registration method[20]. Some of these works address subsurface shift by using the sparse surface measurements to drive finite element models while some provide updated information through overlays on the surface of the MR[15]. Although the largest amount of shift error occurs on the surface, having accurate updated subsurface information would be important in surgical decisions to delineate the remainder of tumor margin after resection.

The same reasons that make biomechanical models the methodology of choice with intraoperative MR, make it a viable avenue to pursue with sparse intraoperative data to obtain subsurface shift information. Skrinjar et. al. compared a damped spring mass model and a linear elastic model for use in conjunction with their stereoscopic camera data, and found that the continuum model was preferable because the spring damping model was mesh dependant on model parameters and lacked a good model guidance strategy[14]. Although physics of brain deformation with loads similar to that applied during surgery, has been studied with hyperviscoelastic models, due to their complexity and computational cost, their feasibility of use for model guided surgical system update has not been adequately demonstrated. Paulsen et. al. used a biphasic model to describe the brain shift in the OR[21]. This model was originally developed by Biot to explain soil mechanics by treating it as a porous medium[22]. In a manner similar to the soil consolidation, it treats the brain tissue as consisting of two distinct phases. The elastic deformations of the solid phase and the pressure gradients of the fluid phase are coupled together. Miga et. al. demonstrated the applicability of this work to gravity induced brain shift in the OR[23]. This model was purely predictive and the sparse data was used for validating the model results. The actual model was driven by simulated forces in the OR such as gravity, pressure gradients caused by hyperosmolar medication, edema etc. These forces are very challenging to measure intraoperatively and cannot be predicted with precision before the surgery. In order to account for this uncertainty, atlas based methods have recently been developed. In their work, Dumpuri et. al. built an atlas of solutions that accounted for shift caused by gravity, edema, and mannitol with different head orientations and capillary permeabilities[24]. The inverse solution was then reconstructed by minimizing the least squared error between the solutions and the measurements made with sparse data. This method was validated with postoperative MR data and the predictions were found to work well with the surface and subsurface measurements. It was noted that the deformations measured intraoperatively are often larger than the postoperative displacements because an estimated 25% shift recovery happens in the period between the surgery and time the postoperative scans are performed. While the surface error for intraoperative data can be validated with sparse measurements, evaluation of subsurface accuracy of the model is more challenging to assess. Nevertheless, some consistent observations have been made about subsurface shift in previous literature. Ferrant et. al. found that the greatest subsurface error in the model lied at the mid-sagittal plane, the location of the rigid membrane, falx cerebri[11]. Other studies in intraoperative MR have shown that relatively little deformation is observed in the regions around the midline, tentorium and contralateral hemisphere[25]. Dura, the outermost meningeal layer, reflects inwards in four places in the brain forming the falx cerebri, tentorium cerebelli, falx cerebelli and diaphragma sellae. These strong structures support the brain parenchyma, preventing large deformation in the contralateral hemisphere, hindbrain and midbrain. The modeling of the falx cerebri was described in Miga et. al.[26] and utilized in Dumpuri et. al.[24, 27] for the atlas based model. This work builds upon the previous study by including a similarly modeled structure for the tentorium cerebelli. The goal of this work is to systematically study the effect of the dural septa on subsurface brain shift and assess the need to model these structures.

2. METHODS

2.1. Data acquisition

Preoperative MR tomograms were acquired for three patients using a 1.5 T clinical scanner a day prior to undergoing tumor surgery. The acquired images were T1 weighted and gadolinium enhanced with voxel size of 1mm × 1mm × 1.2mm. The first patient was 22 year old female with a grade II oligodendroglioma in the left frontal lobe. The second patient was 58 year old male with a metastatic tumor in the left parietal hemisphere. The third patient was a 77 year old male with glioblastoma multiforme in the left temporal hemisphere. Sparse intraoperative data was also collected for these patients. Patient consent was obtained prior to surgery for this Vanderbilt Institutional Review Board approved procedure. A commercial LRS device (RealScan3D USB, 3D Digital Corp, Bethel, CT) was used to obtain scans after the craniotomy and opening the dura and after tumor resection. The scanner was outfitted with infrared emitting diodes and its position was tracked in the OR. The scanning device can obtain textured surfaces via a camera that measures a triangulated laserline sweep and a Canon Optix 400 camera that acquires texture information.

2.2. Mesh construction

Patient specific meshes were created individually from MR images. Brain and tumor surfaces were created from manually segmented isointensity images using the marching cube algorithm[28] and smoothed using the Laplacian smoothing function[29]. Tetrahedral elements were used to construct the mesh. The edge length of the element was ~5 mm and refinement was performed around the tumor surface. Usually this resulted in ~20,000 nodes and ~100,000 elements. An intensity threshold was then used to classify the brain parenchyma elements as being gray matter or white matter.

Falx cerebri is a rigid dural membrane in the mid-sagittal plane, that separates the left and the right forebrain regions. It was segmented and meshed in a manner similar to that described in Miga et. al.[26] and utilized in Dumpuri et. al.[24, 27] The falx was segmented from the sagittal view of the image and nodes within that perimeter were used to split a plane in the mesh. This procedure is shown in Figure 1 below.

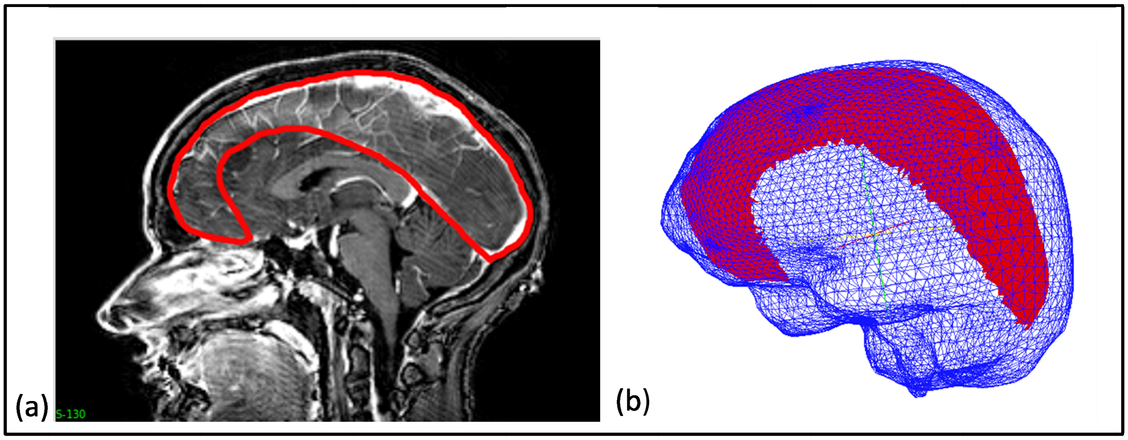

Figure 1: Falx segmentation procedure. (a) manual periphery drawn around falx on gadolinium enhanced MRI (b) segmented falx overlaid with the mesh.

The invagination of the dura in the tentorium region encloses the straight sinus which shows up as a high intensity region in gadolinium enhanced images. Three points were selected in this region and used to clip a plane along the brain mesh. This plane was manually segmented into an approximate tentorium shaped structure. Several evenly distributed points were selected on the contrast enhanced images in the tentorium region. Closest distance points were found on the previously segmented plane. These two sets of points were used as target points and control points in a 3D thin plate spline algorithm to morph the manually segmented plane into a tentorium surface, which was then smoothed. The tentorium cerebelli in the contralateral hemisphere was segmented similarly. Those surfaces were used to create tentorium nodes in the finite element mesh. This procedure is demonstrated in Figure 2 below.

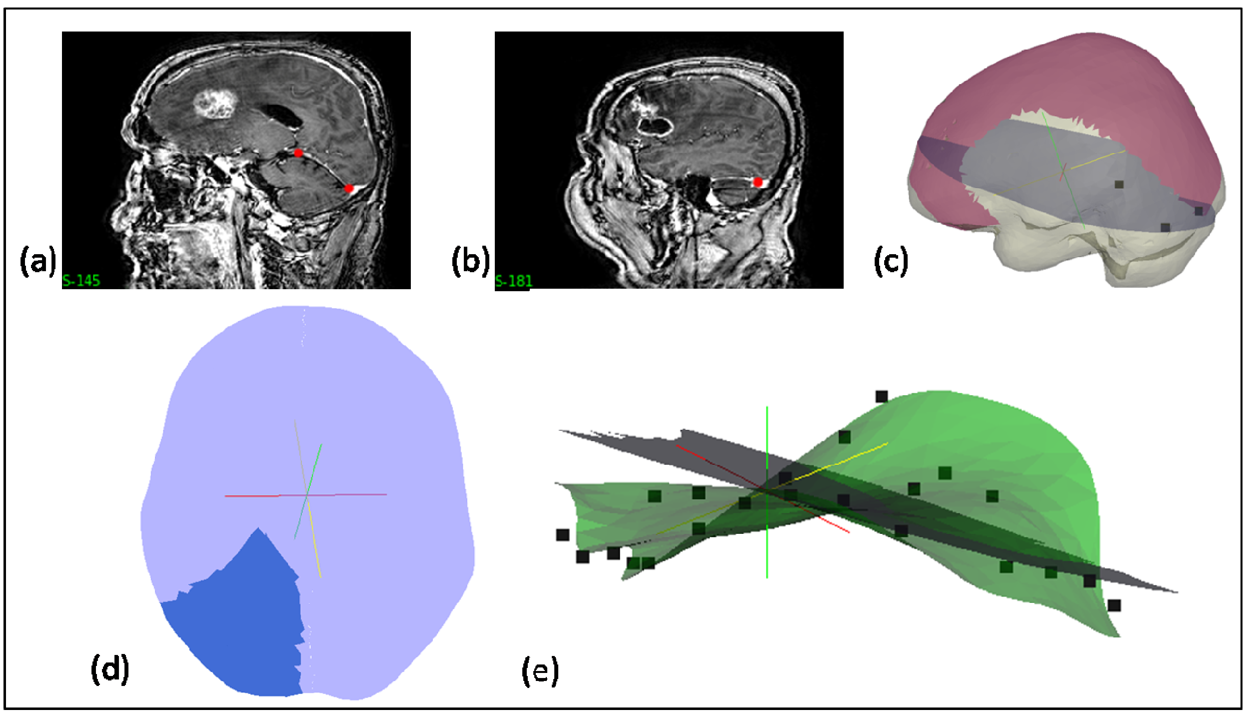

Figure 2: Procedure for tentorium segmentation. (a) and (b) show the selection of three points used for clipping a plane in the mesh, (c) shows the clipped plane (with those three points) overlaid with the mesh and the falx, (d) shows the clipped plane segmented into an approximate tentorium shaped structure and (e) shows the segmented plane with the final tentorium surface created by morphing the plane in (d) using a thin plate spline algorithm. The points on the surface are the target points used to drive the thin plate spline algorithm.

The quality of the segmentation was assessed visually by overlaying the tentorium points on the gadoliunium enhanced images.

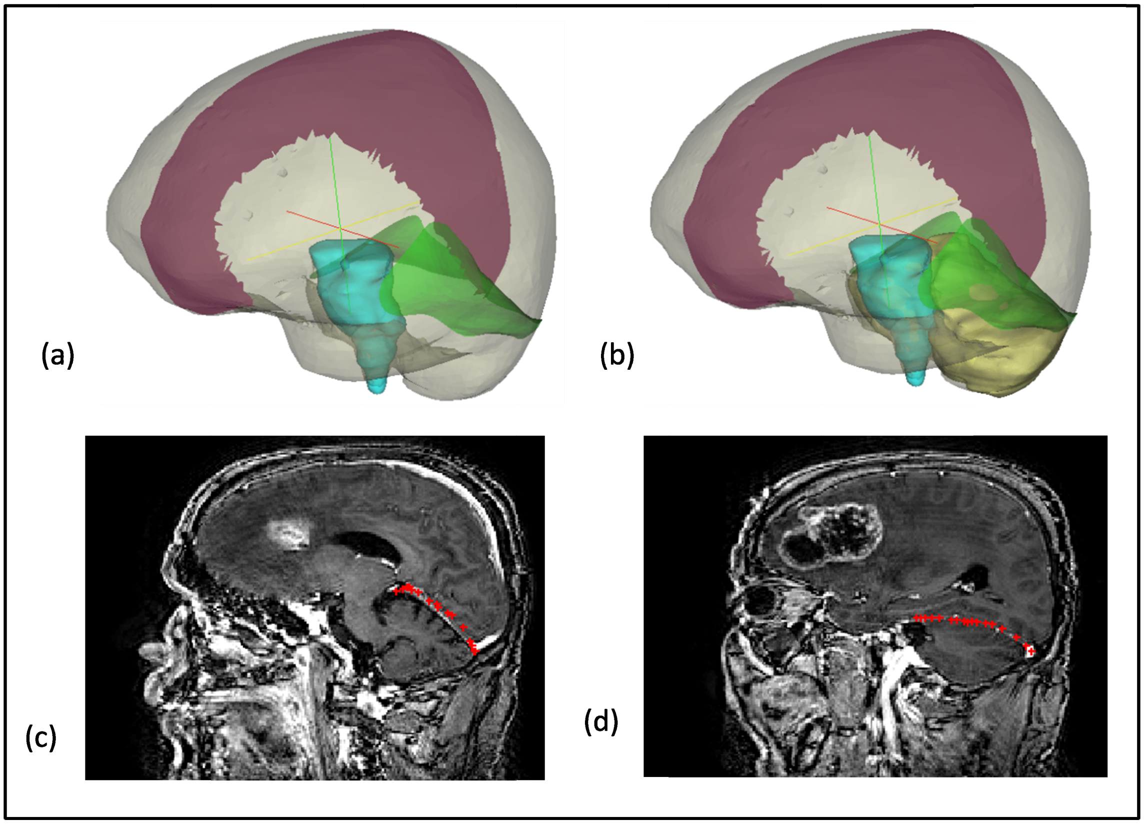

Figure 3: Results of falx and tentorium segmentation. (a) and (b) shows the mesh overlaid with the falx and the tentorium surfaces. The segmented brainstem (in blue) in figure (a) and cerebellum (in yellow) in figure (b) are shown for reference, were not modeled separately. (c) and (d) are two saggital MRI slices overlaid with the red points of the tentorium surface. A good overlap of the points and the hyperintense region indicate the quality of segmentation.

Figure 3(c) shows a medial slice whereas Figure 3(d) shows a lateral slice. The overlay for the medial slice is slightly inaccurate, however the overall patient specific representation of the tentorium is fairly good for modeling purposes.

2.3. Computational model

The biphasic model proposed by Miga et. al. was used to model the shift deformations[23]. The model was set up in a way very similar to that described in Dumpuri et. al.[24] and the details are provided here for completeness. The equations of biphasic consolidation are listed below:

$$\nabla \cdot G\nabla\vec{u} + \nabla\frac{G}{1-2\nu}\left(\nabla\cdot\vec{u}\right) - \alpha\nabla p = -\left(\rho_t - \rho_f\right)g \tag{1}$$

$$\alpha\frac{\partial}{\partial t}\left(\nabla\cdot\vec{u}\right) + \frac{1}{S}\frac{\partial p}{\partial t} + k_c\left(p - p_c\right) = \nabla\cdot k\nabla p \tag{2}$$

The term $\vec{u}$ is the displacement vector, p is the interstitial pressure, G is the shear modulus, ν is the Poisson's ratio, α is the ratio of fluid volume extracted to volume change of the tissue under compression, ρ_t is the tissue density, ρ_f is the fluid density, g is the gravitational unit vector, $1/S$ is the amount of fluid that can be forced into a tissue under a constant volume, t is the time, k_c is the capillary permeability, p_c is the intracapillary pressure, and k is the hydraulic conductivity. The material properties were also used as stated in Dumpuri et. al.[24]

Two kinds of deformation were simulated: deformation caused by gravity and deformation caused by mannitol, a hyperosmolar drug administered prior to surgery to reduce intracranial pressure. The boundary conditions used for running the simulations are similar to those used in Dumpuri et al.[27] Three different displacement boundary conditions were used- fixed, stress free, and slippage. The brainstem is fixed and experiences no deformation. The highest region on the head, according to the head orientation, is designated to be stress free. All other nodes on the boundary, including the internal boundaries (the falx cerebri and the tentorium cerebelli), are assigned slip boundary conditions, that is, they cannot move in the normal direction, but movement in the tangential direction is permitted. The demarcation between the stress free and no slippage region is done according to the head orientation, the demarcating plane is perpendicular to the direction of gravity and its level is set empirically. The pressure boundary conditions were set by the presumed level to which cerebrospinal fluid has drained during the procedure. The nodes exposed to atmospheric pressure have a Dirichlet boundary condition and the nodes submerged in fluid are subject to Neumann boundary conditions of zero flux across. Tissue resection was simulated by decoupling nodes belonging to tumor material type. The above analysis was performed on two different meshes for each patient- one that contained the dural septa and one that didn't. For each mesh, the gravity and mannitol atlases were built separately. The gravity atlas consisted of 60 different head orientations, each with three different levels of fluid drainage, simulated either with or without tissue resection- resulting in 360 total solutions. The mannitol atlas consisted of 60 head orientations as well, three different capillary permeability values, simulated either with or without tissue resection- also resulting in 360 total solutions. In addition, atlases constructing by concatenating the two atlases were also analyzed.

The atlas of displacement solutions computed above are compiled into a matrix *E* that consists of *3N* rows and m columns, where *N* is the number of nodes in the mesh (with each node having a displacement solution in the Cartesian x, y, and z directions) and *m* is the number of solutions in an atlas. The sum of squared error between the inverse solution and the true solution is defined as following.

$$\varepsilon = \left(E\boldsymbol{\alpha} - \boldsymbol{U}\right)^T \left(E\boldsymbol{\alpha} - \boldsymbol{U}\right) \tag{3}$$

In equation (3), □ is a sum of squared error between the inverse solution ($E\boldsymbol{\alpha}$ term) and the true solution (second term, $\boldsymbol{U}$). *E* is the matrix of atlas solutions and $\boldsymbol{\alpha}$ is an $m \times 1$ vector of weighting coefficients. The weighting coefficients can be obtained by the least squared error approach.

$$\boldsymbol{\alpha} = \left(E^T E\right)^{-1} E\boldsymbol{U} \tag{4}$$

Since the true solution over the entire domain is unknown, only sparse solutions are available, the above equation is rewritten as following.

$$\boldsymbol{\alpha} = \left(M^T M\right)^{-1} M\boldsymbol{u}_{sparse} \tag{5}$$

In equation 5, *M* is the matrix of sparse atlas solutions which is $3n_s$ rows and m columns, n_s being the number of sparse points or previously computed homologous points on the LRS surfaces, where the deformation is known from the tracking of the pre and post resection LRS. $\boldsymbol{u}_{sparse}$ is an $3n_s$ vector of those measured displacements. However equation (5) is an ill-posed problem. The first term in equation (5) is singular because the number of atlas solutions far exceeds the number of sparse homologous points. This can be resolved by a constrained linear optimization approach.

$$\min \left\| M\boldsymbol{\alpha} - \boldsymbol{u}_{sparse} \right\|^2 \ni \ 0 \le \alpha_i \le 1 \text{ and } \sum_{i=1}^{m} \alpha_i \le 1 \tag{6}$$

The first constraint ensures that all the weighting coefficients are positive. Hence if a solution in an atlas deforms in the incorrect direction, the objective function would weigh that solution lower instead of assigning a higher negative regression coefficient. The second constraint ensures that the solution is always interpolated, and not extrapolated. The implementation of the method of Lagrange multipliers in the Optimization Toolbox of MATLAB® (Mathworks Inc) was used to solve this linear constrained least squared error problem.

3. RESULTS

Shift was measured across three cases through homologously selected points on registered pre and post resection LRS images. The average and maximum magnitude of measured shifts for each of the patients at the homologous points are listed in Table 1.

Table 1: The number of homologous points and average and maximum of the measured displacements.

#	# measurement points	Average shift ± standard deviation (mm)	Maximum shift (mm)
1	16	22.89±6.29	28.93
2	24	6.76±2.43	10.49
3	18	8.58±0.60	9.66

Percentage shift correction was measured using the formulation listed in Dumpuri et. al.[24]

$$Shift\ correction = 1 - \frac{Shift\ error}{Shift\ magnitude} \tag{7}$$

These shift recoveries for all patients using the simulations with two different meshes are shown in Figure 4.

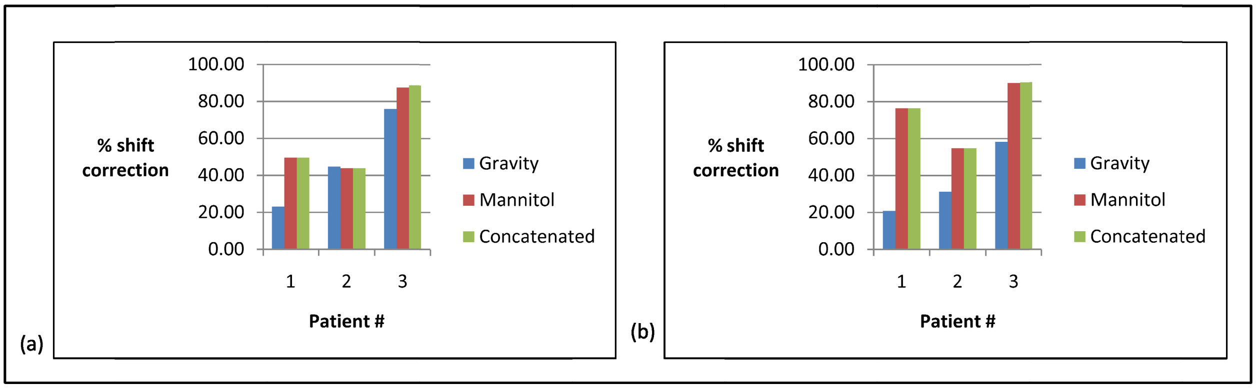

Figure 4: Shift recoveries- (a) Mesh without membranes and (b) mesh with membranes.

Shift correction for most cases is higher for the mannitol solutions than the gravity solutions. When analogous solutions are compared across the two different meshes- the mesh with and without membranes, the shift corrections are pretty similar for each case. The model corrected images for the two of the three cases are shown in Figure 5 below.

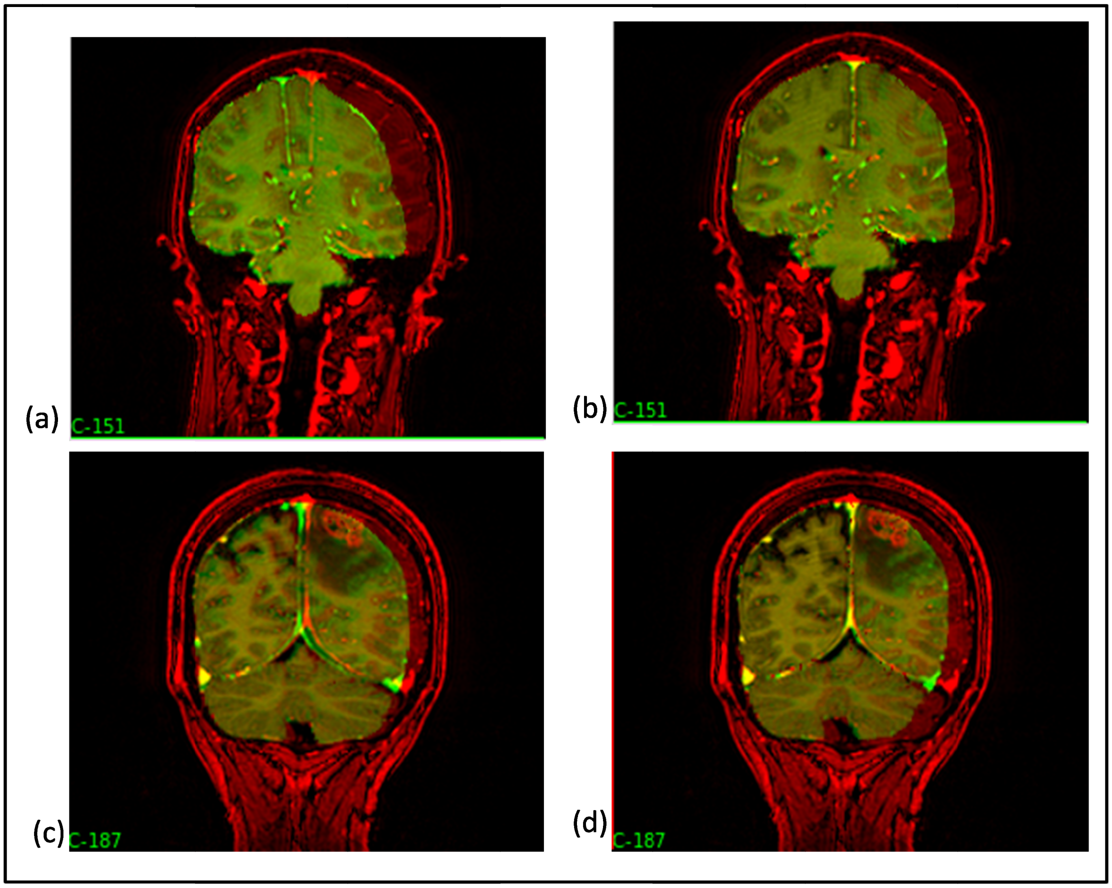

Figure 5: Preoperative image (red) overlaid with model deformed image (green) for the mannitol solutions the (a) mesh without membrane for Patient 1, (b) the mesh with membranes for Patient 1, (c) mesh without membrane for Patient 2 and (d) the mesh with membranes for Patient 2.

The concatenated atlases were used to deform the images. The hyperintense regions in the center of the image represent the sinuses enclosed in the dural membranes. For the mesh without the membranes, there is considerable movement in the position of the falx, whereas the midline stays fairly steady for the mesh with the membrane. The movement in the midline is greater for Patient 1 without membranes than Patient 2 without membranes because the overall shift is much higher. The differences in the positions of the centroid of the tumor after deformation in the mesh with and without the membranes are shown in Table 2 below.

Table 2: The difference in the position of the centroid of the tumor nodes in the meshes with and without the membranes

#	**Difference in position (mm)**
1	4.16
2	1.10
3	0.86

The computations were done with the reconstructed solutions from the concatenated atlases. The centroid of the tumor nodes are predicted to be in different positions depending on whether membranes were modeled. To examine the difference in subsurface shift, the magnitude of the vector difference between the displacement vectors was studied at the tumor boundary, close to the falx region, close to the tentorium region and over the entire domain. The probability density functions of the vector difference at those four regions for Patient #3 are shown in Figure 6 below.

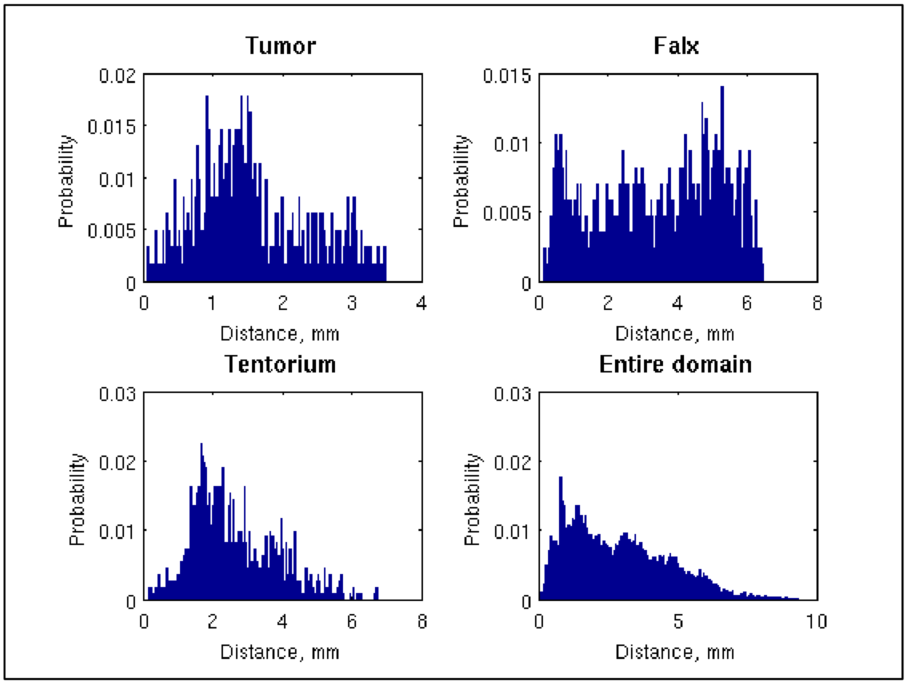

Figure 6: Probability density functions of the magnitude of the vector difference for predicted displacements for Patient #3 with and without membranes in the following regions- tumor boundary, close to falx, close to tentorium and the entire domain. The x-axis represent the vector displacement in mm and the y-axis represents the probabilities.

The above probability density functions demonstrate the difference in the predicted subsurface shifts for the mesh with and without the dural septa. While the predicted percentage shift corrections were pretty similar for both the meshes in this patient, the predicted subsurface shift can differ by a few millimeters in the regions around the tumor boundary, falx and tentorium.

4. DISCUSSION

Overall, the best shift corrections were observed in the mannitol atlases for the mesh with the membrane. When the dural septa are accounted for in the model, the subsurface deformations are also in greater compliance with the observations made in previous literature. Maurer et. al. observed that the deformation was very small in the midline, tentorial, and contralateral hemisphere regions[25] and Ferrant et. al. noted that the largest errors in model predictions were seen in the midline region[11]. For the three cases presented here, improvements in surface shift were observed to different extents for all cases. The subsurface shifts were also qualitatively different for these cases, as seen in Figure 5. Smaller deformations were observed in the regions of falx and tentorium when those membranes were modeled. Some quantitative difference was also seen in the tumor centroid predictions in Table 2. Lack of intraoperative MR data makes it difficult to perform a comparison of the true subsurface shifts. Overall, the studies presented for the cases above provide a strong support for the need to account for the membranes in the model.

Another interesting observation is the shift corrections predicted by various mechanisms. The mannitol atlases outperform the gravity solutions for all three cases for the mesh with membranes. The magnitude of shift predicted by gravity is smaller than that predicted by mannitol. Before the craniotomy and any CSF drainage, mannitol has already been administered to the patient. In the OR environment, various forces- gravity, mannitol, edema, tissue resection- act concurrently on the brain and it is difficult to sequester the contribution of each of these forces individually. Also, the complexity of the cerebrospinal fluid system may not be well reflected in the current model for gravity, which is modeled as a buoyancy force acting by the rising or falling of the fluid line. In addition to surrounding the external surface of the brain parenchyma, this fluid is present in a continuous space in the sinuses and the ventricles. The segmented surface of the brain is also smoother whereas in reality the brain surface contains many crevices and fissures that are fluid filled, and removal of fluid from those cavities would cause a greater amount of shift than is predicted by the current model of gravity. However, this study should not be taken as conclusive evidence of the proportion of the contributions of various physical forces acting on the brain tissue during surgery.

The fidelity of an intra-operative guidance system in neurosurgery is compromised due to shift in the OR caused by various factors such as gravity, hyperosmolar drugs, edema. A considerable body of work in literature has focused on solving this problem through intraoperative imaging or updating preoperative images with mathematical models. Most volumetric intra-operative imaging modalities used for updated information in the OR suffer from shortcomings such as high cost, exposure to radiation, lower contrast, and most importantly loss of information acquired in the pre-operative MR. In order to preserve the rich stream of information acquired preoperatively, such as contrast agent imaging studies, fiber tracking studies, functional information, there has been a move in the recent literature to update the pre-operative images to reflect the changes caused by the non-rigid deformation. The more cost efficient alternative to volumetric intraoperative imaging modalities that have been explored in past are strereoscopic camera devices and laser range devices, both of which provide sparse surface data in the OR. This paper builds upon the previous work of Dumpuri et. al.[24, 27] where an atlas of solutions was used in order to compensate for the inherent uncertainty in the OR. A novel method of segmenting and modeling the two major dural membranes- falx cerebri and tentorium cerebelli was described and systematically studied. In future work, the modeling of falx and tentorium would be tested on more patient data to derive statistical trends from the data.

ACKLNOWLEDGEMENTS

This work was supported by the NIH-National Institute for Neurological Disorders and Stroke - Grant # R01 NS049251-01A4.

REFERENCES

[1] Nauta, H. J., "Error assessment during "Image guided" And "Imaging interactive" Stereotactic surgery," Comput Med Imaging Graph 18(4), 279-87 (1994).
[2] Hill, D. L. G., Maurer, C. R., Maciunas, R. J., Barwise, J. A., Fitzpatrick, J. M. and Wang, M. Y., "Measurement of intraoperative brain surface deformation under a craniotomy," Neurosurgery 43(3), 514-526 (1998).
[3] Nimsky, C., Ganslandt, O., Cerny, S., Hastreiter, P., Greiner, G. and Fahlbusch, R., "Quantification of, visualization of, and compensation for brain shift using intraoperative magnetic resonance imaging," Neurosurgery 47(5), 1070-1079 (2000).
[4] Roberts, D. W., Hartov, A., Kennedy, F. E., Miga, M. I. and Paulsen, K. D., "Intraoperative brain shift and deformation: A quantitative analysis of cortical displacement in 28 cases," Neurosurgery 43(4), 749-758 (1998).
[5] Kelly, P. J., "Intraoperative brain shift and deformation: A quantitative analysis of cortical displacement in 28 cases - comment," Neurosurgery 43(4), 759-759 (1998).
[6] Butler, W. E., Piaggio, C. M., Constantinou, C., Nikalson, L., Gonzales, R. G., Cosgrove, G. R. and Zervas, N. T., "A mobile computed tomographic scanner with intraoperative and intensive care unit applications.," Neurosurgery 88(4), 1304-1310 (1998).
[7] Letteboer, M. M. J., Willems, P. W. A., Viergever, M. A. and Niessen, W. J., "Brain shift estimation in image-guided neurosurgery using 3-d ultrasound," IEEE Transactions on Biomedical Engineering 52(2), 268-276 (2005).
[8] Archip, N., Clatz, O., Whalen, S., Kacher, D., Fedorov, A., Kot, A., Chrisocholdes, N., Jolesz, F., Golby, A., Black, P. M. and Warfield, S. K., "Non-rigid alignment of pre-operative mri, fmri, and dt-mri with intra-operative mri for enhanced visualization and navigation in image-guided neurosurgery," Neuroimage 35(2), 609-624 (2007).
[9] Hata, N., Dohi, T., Warfield, S. K., Wells, I., W.M., Kikinis, R. and Jolesz, F. A., "Multimodality deformable registration of pre- and intraoperative images for mri-guided brain surgery," Proceedings of the First International Conference on Medical Image Computing and Computer-Assisted Intervention 1496(1998), 1067-1074 (1998).
[10] Hagemann, A., Rohr, K., Stiehl, H. S., Spetzger, U. and Gilsbach, J. M., "Biomechanical modeling of the human head for physically based, nonrigid image registration," IEEE Transactions on Medical Imaging 18(10), 875-884 (1999).
[11] Ferrant, M., Nabavi, A., Macq, B. t., Jolesz, F. A., Kikinis, R. and Warfield, S. K., "Registration of 3-d intraoperative mr images of the brain using a finite-element biomechanical model," IEEE Transactions on Medical Imaging 20(12), 1384 (2001).

[12] Wittek, A., Miller, K., Kikinis, R. and Warfield, S. K., "Patient-specific model of brain deformation: Application to medical image registration," Journal Of Biomechanics 40(4), 919-929 (2007).
[13] Clatz, O., Delingette, H., Talos, I.-F., Golby, A. J., Kikinis, R., Jolesz, F., Ayache, N. and Warfield, S., "Robust non-rigid registration to capture brain shift from intraoperative mri," IEEE Transactions on Medical Imaging 24(11), 1417-1427 (2006).
[14] Skrinjar, O., Nabavi, A. and Duncan, J., "Model-driven brain shift compensation," Medical Image Analysis 6(4), 361-373 (2002).
[15] Sun, H., Roberts, D. W., and Farid, H., Wu, Z., Hartov, A. and Paulsen, K. D., "Cortical surface tracking using a stereoscopic operating microscope," Neurosurgery 56(1), 86-97 (2005).
[16] Audette, M. A., Siddiqi, K., Ferrie, F. P. and Peters, T. M., "An integrated range-sensing, segmentation and registration framework for the characterization of intra-surgical brain deformations in image-guided surgery," Computer Vision and Image Understanding 89(2-3), 226-251 (2003).
[17] Sinha, T. K., Miga, M. I., Cash, D. M. and Weil, R. J., "Intraoperative cortical surface characterization using laser range scanning: Preliminary results," Neurosurgery 59(4), 368-376 (2006).
[18] Cao, A., Thompson, R. C., Dumpuri, P., Dawant, B. M., Galloway, R. L., Ding, S. and Miga, M. I., "Laser range scanning for image-guided neurosurgery: Investigation of image-to-physical space registrations," Medical Physics 35(4), 1593-1605 (2008).
[19] Sinha, T. K., Dawant, B. M., Duay, V., Cash, D. M., Weil, R. J. and Miga, M. I., "A method to track cortical surface deformations using a laser range scanner," IEEE Transactions on Medical Imaging 24(6), 767-781 (2005).
[20] Ding, S., Miga, M. I., Noble, J. H., Cao, A., Dumpuri, P., Thompson, R. C. and Dawant, B. M., "Semiautomatic registration of pre- and postbrain tumor resection laser range data: Method and validation," Biomedical Engineering, IEEE Transactions on 56(3), 770-780 (2009).
[21] Paulsen, K. D., Miga, M. I., Kennedy, F. E., Hoopes, P. J., Hartov, A. and Roberts, D. W., "A computational model for tracking subsurface tissue deformation during stereotactic neurosurgery.," IEEE Transactions on Biomedical Engineering 49(8), 823-835 (1999).
[22] Biot, M. A., "General theory of three-dimensional consolidation," Journal of Applied Physics 12(2), 155-164 (1941).
[23] Miga, M. I., Paulsen, K. D., Lemery, J. M., Eisner, S. D., Hartov, A., Kennedy, F. E. and Roberts, D. W., "Model-updated image guidance: Initial clinical experiences with gravity-induced brain deformation," IEEE Transactions on Medical Imaging 18(10), 866-874 (1999).
[24] Dumpuri, P., Thompson, R. C., Dawant, B. M., Cao, A. and Miga, M. I., "An atlas-based method to compensate for brain shift: Preliminary results," Medical Image Analysis 11(2), 128-145 (2006).
[25] Maurer, C. R., Hill, D. L. G., Martin, A. J., Liu, H., McCue, M., Rueckert, D., Lloret, D., Hall, W. A., Maxwell, R. E., Hawkes, D. J. and Truwit, C. L., "Investigation of intraoperative brain deformation using a 1.5t interventional mr system: Preliminary results.," IEEE Transactions on Medical Imaging 17(5), 817-825 (1998).
[26] Miga, M. I., Paulsen, K. D., Kennedy, F. E., Hartov, A. and Roberts, D. W., "Model-updated image-guided neurosurgery using the finite element method: Incorporation of the falx cerebri," Proceedings of the Second International Conference on Medical Image Computing and Computer-Assisted Intervention (1999).
[27] Dumpuri, P., Thompson, R. C., Cao, A., Ding, S., Garg, I., Dawant, B. M. and Miga, M. I., "A fast efficient method to compensate for brain shift for tumor resection therapies measured between preoperative and postoperative tomograms.," IEEE Transactions on Biomedical Engineering in press), (2010).
[28] Lorensen, W. E. and Cline, H. E., "Marching cubes: A high resolution 3d surface construction algorithm," SIGGRAPH Comput. Graph. 21(4), 163-169 (1987).
[29] Schroeder, W. J., Martin, K. M. and Lorensen, W. E., [Visualization toolkit: An object-oriented approach to 3d graphics], Kitware, Inc, 331-334 (2003).